THE JOURNAL OF BIOLOGICAL CHEMISTRY
Vol. 276, No. 45, Issue of November 9, pp. 42099–42107, 2001

Printed in U.S.A.

Structure Prediction and Active Site Analysis of the Metal Binding Determinants in γ-Glutamylcysteine Synthetase*

Received for publication, May 23, 2001, and in revised form, August 13, 2001
Published, JBC Papers in Press, August 29, 2001, DOI 10.1074/jbc.M104672200

Jared J. Abbott‡§¶, Jimin Pei§‖, Jennifer L. Ford‡, Yuan Qi‖, Vyacheslav N. Grishin‖, Lisa A. Pitcher‡, Margaret A. Phillips‡, and Nick V. Grishin‖‡‡**

From the Departments of ‡Pharmacology and ‖Biochemistry and the ‡‡Howard Hughes Medical Institute, University of Texas Southwestern Medical Center, Dallas, Texas 75390-9041

γ-Glultamylcysteine synthetase (γ-GCS) catalyzes the first step in the *de novo* biosynthesis of glutathione. In trypanosomes, glutathione is conjugated to spermidine to form a unique cofactor termed trypanothione, an essential cofactor for the maintenance of redox balance in the cell. Using extensive similarity searches and sequence motif analysis we detected homology between γ-GCS and glutamine synthetase (GS), allowing these proteins to be unified into a superfamily of carboxylate-amine/ammonia ligases. The structure of γ-GCS, which was previously poorly understood, was modeled using the known structure of GS. Two metal-binding sites, each ligated by three conserved active site residues (n1: Glu-55, Glu-93, Glu-100; and n2: Glu-53, Gln-321, and Glu-489), are predicted to form the catalytic center of the active site, where the n1 site is expected to bind free metal and the n2 site to interact with MgATP. To elucidate the roles of the metals and their ligands in catalysis, these six residues were mutated to alanine in the *Trypanosoma brucei* enzyme. All mutations caused a substantial loss of activity. Most notably, E93A was able to catalyze the L-Glu-dependent ATP hydrolysis but not the peptide bond ligation, suggesting that the n1 metal plays an important role in positioning L-Glu for the reaction chemistry. The apparent K_m values for ATP were increased for both the E489A and Q321A mutant enzymes, consistent with a role for the n2 metal in ATP binding and phosphoryl transfer. Furthermore, the apparent K_d values for activation of E489A and Q321A by free Mg^{2+} increased. Finally, substitution of Mn^{2+} for Mg^{2+} in the reaction rescued the catalytic deficits caused by both mutations, demonstrating that the nature of the metal ligands plays an important role in metal specificity.

Glutathione (γ-glutamyl-cysteinyl-glycine) is a tripeptide thiol that acts as a sulfhydryl buffer. It is present in mammalian cells at high concentrations and plays an important role in many cellular processes, such as detoxification of oxidative species, protein and DNA synthesis, and cellular import of amino acids (1, 2). The parasitic protozoa *Trypanosoma brucei* causes African sleeping sickness, a disease responsible for significant morbidity and mortality in Africa. The identification of metabolic differences between parasite and host is an important step in the development of new anti-trypanosomal agents (3). Mammals and trypanosomes differ in their metabolism of glutathione. Trypanosomes utilize a unique molecule that is a conjugate of glutathione and spermidine, called trypanothione, to maintain reduced thiol pools in the cell (4). The first committed step in the biosynthesis of glutathione, and thereby trypanothione, is the formation of γ-glutamylcysteine, catalyzed by γ-glutamylcysteine synthetase (γ-GCS)[1] (5). γ-GCS is the rate-limiting enzyme in the synthesis of glutathione in mammalian cells (6) and of trypanothione in the trypanosomatid, *Leishmania tarentolae* (7).

γ-GCS catalyzes the formation of a peptide bond between the γ-carboxyl of L-Glu and the α-amino group of L-Cys. A number of acceptor amino acids have been tested in place of L-Cys and the enzyme was found to catalyze the reaction utilizing L-Aba with similar efficiency as L-Cys (8). The enzyme utilizes ATP to promote this reaction by first phosphorylating the γ-carboxyl of L-Glu (Fig. 1). The phosphate group of this intermediate is a good leaving group for the subsequent attack by the α-amino group of L-Cys (5). Purified rat kidney γ-GCS is activated by both Mg^{2+} and Mn^{2+} (9). Mn^{2+} activates the enzyme at 10-fold lower concentrations than Mg^{2+}, but the rate in the presence of Mn^{2+} is 4-fold slower than with Mg^{2+}. Moreover, Mn^{2+} lowers the specificity of the enzyme for the acceptor amino acid (8).

γ-GCS has been identified in animals, bacteria, plants, fungi, and protozoa. However, the relationship between animal, bacterial, and plant enzymes was unclear due to the absence of pronounced sequence similarity between them (10). Despite extensive functional studies of γ-GCS in many organisms, our understanding of its structure and catalytic mechanism had been limited. A three-dimensional structure of γ-GCS is not available and the enzyme is structurally unrelated to mechanistically similar enzymes such as D-Ala D-Ala ligase and glutathione synthetase (11). However, with the rapid expansion of protein sequence data and the development of sensitive similarity search tools such as PSI-BLAST (12) and HMMer (13), the limits of sequence-based homology detection are being extended (14). Multiple sequence alignments contain information about the positional variation of amino acid usage that is the basis for profile generation (15). Profiles transformed into po-

* This work was supported in part by National Institutes of Health Grants R01AI34432 (to M. A. P.) and T32-GM08014 (to J. J. A.) and Welch Foundation Grants I-1257 (to M. A. P.) and I-1505 (to N. V. G.). The costs of publication of this article were defrayed in part by the payment of page charges. This article must therefore be hereby marked "*advertisement*" in accordance with 18 U.S.C. Section 1734 solely to indicate this fact.

§ Contributed equally to the results of this work.

¶ Medical Scientist Training Program.

** Recipient of a Burroughs Wellcome Fund Scholar Award in Molecular Parasitology. To whom correspondence should be addressed. Tel.: 214-648-3637; Fax: 214-648-9961; E-mail: margaret.phillips@utsouthwestern.edu.

[1] The abbreviations used are: γ-GCS, γ-glutamylcysteine synthetase; GS, glutamine synthetase; L-Aba, L-α-aminobutyrate; MOPS, 4-morpholinepropanesulfonic acid; HPLC, high performance liquid chromatography; mutant enzymes are designated by single amino acid codes and residue number, *eg*. E55A, Glu-55 to Ala mutant *T. brucei* γ-GCS.

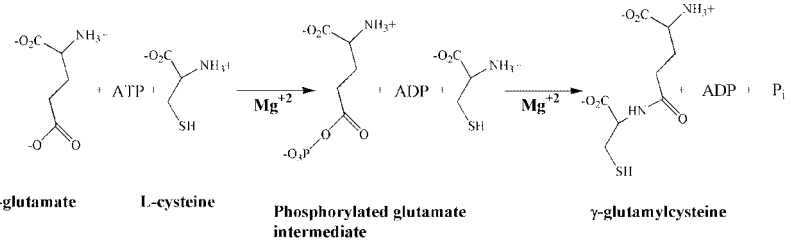

FIG. 1. **The proposed reaction mechanism of γ-GCS catalyzed peptide bond ligation.**

sition-specific scoring matrices (12, 16) or encoded in hidden Markov models (17) enhance the sensitivity of sequence similarity searches.

In the course of extensive similarity searches using PSI-BLAST (12), we were able to detect homology between animal, fungal, plant, and bacterial γ-GCS proteins. A multiple alignment was constructed from these γ-GCS sequences. Using the profile generated from this multiple sequence alignment, statistically significant sequence similarity between γ-GCS and glutamine synthetase (GS) was found. Homology between γ-GCS and GS was further supported by secondary structure predictions and conservation pattern analysis.

GS is a crucial enzyme in nitrogen metabolism that ligates ammonia to the γ-carboxyl of L-Glu, also in an ATP-dependent reaction (18, 19). The structure of GS with and without bound substrates has been reported (20) and thus provides a fold prediction for γ-GCS that yields insight into the molecular basis of its catalytic function. A partial model of the γ-GCS active site was constructed based on the GS structure allowing the Mg^{2+}, MgATP, and L-Glu-binding sites to be modeled.

This model of the γ-GCS active site residues was used as a guide for experimental studies of the *T. brucei* γ-GCS, which has previously been kinetically characterized (21, 22). Based on the homology to GS, six conserved residues in γ-GCS are predicted to form two metal-binding sites (n1: Glu-55, Glu-93, Glu-100; and n2: Glu-53, Glu-489, Gln-321). The roles of these six amino acid residues were probed by site-directed mutagenesis. All six residues are crucial for enzyme activity. The activity of only three of the mutant enzymes (E93A, E489A, and Q321A) was sufficient for detailed study. E93A was able to catalyze L-Glu-dependent ATP hydrolysis but not peptide bond ligation, suggesting that the n1 metal plays an important role stabilizing the transition state for this latter step. Mutations of Glu-489 and Gln-321 to Ala greatly affected both metal activation and MgATP binding, supporting a role for the n2 metal in binding of MgATP. Surprisingly, we found that Mn^{2+} can rescue activity in these mutants. These data validate an important structural prediction and provide novel insight regarding the residues in the active site of γ-GCS that are crucial for divalent metal binding and catalysis.

EXPERIMENTAL PROCEDURES

Materials—All reagents for the enzyme assay were purchased from Sigma, Ni^{2+}-agarose and pREP4 were purchased from Qiagen.

Similarity Searches—The PSI-BLAST (12) program was used to search for homologues of γ-GCS family proteins. Complete γ-GCS sequences from fungi (*Saccharomyces cerevisiae*, gi|6322360), plants (*Lycopersicon esculentum*, gi|7489004), and bacteria (*Escherichia coli*, gi|121661) were used as PSI-BLAST queries to search against the non-redundant (nr) data base at NCBI (January 2001, 598, 612 sequences, 189, 197, 841 letters). The E-value threshold was set to 0.05. The BLOSUM62 matrix (23) was used for scoring, and low complexity filtering using the SEG program (24) was applied to the data base sequences but not to the query sequences. Found homologues were grouped by single-linkage clustering (1 bit per site threshold, about 50% identity) as implemented in the SEALS package (25), and the representative sequences from the groups were used as new queries for PSI-BLAST iterations. Representative γ-GCS sequences were also submitted as queries to search against the ERGO data base (igweb.integratedgenomics.com/ERGO/).

Multiple Sequence Alignments—Multiple sequence alignments were constructed using the T-COFFEE program (26) for each γ-GCS sequence group. These alignments were merged manually based on the conservation patterns and secondary structure predictions from the JPRED server (27). The merged multiple sequence alignment was used as input to generate a position-specific scoring matrix (-B option in the program blastpgp (12)) for a new round of PSI-BLAST searches starting from each individual γ-GCS sequence. Multiple alignments for representative sequences of the three types of GSs were also constructed by T-COFFEE (26), adjusted manually and merged with the γ-GCS alignment. The complete full-length alignment is available through anonymous FTP from ftp://iole.swmed.edu/pub/gGCS/gGCS_ali.doc.

Euclidian Space Mapping and Distance Diagram for the γ-GCS and GS Sequences—The conserved segments of the γ-GCS and GS multiple alignment shown in Fig. 2 were used to calculate pairwise identity fractions q_{ij} between each sequence pair i and j. The identity fractions were converted to evolutionary distances with the formula,

$$d_{ij} = -\ln[(q_{ij} - q_{ij}^{ran})/(1 - q_{ij}^{ran})] \quad \text{(Eq. 1)}$$

where q_{ij}^{ran} is an expected identity percentage of two random sequences with the same amino acid composition as the sequences i and j. Each sequence was represented as a point in a multidimensional Euclidian space in such a way that Euclidian distances $\bar{d}_{ij}$ between the points optimally approximated the estimated distances d_{ij} between the sequences,

$$\sum_{ij}(\bar{d}_{ij}^2 - d_{ij}^2)^2/d_{ij}^4 = \min \quad \text{(Eq. 2)}$$

These points were grouped using the following procedure. Each point representing a sequence generated a Gaussian density in the Euclidian space having the following properties. The mean of each density was the point's coordinates and the variance σ^2 of each density was identical for all points. Starting from each point, the local maximum of the sum of such Gaussians was found. The points giving rise to the same local maximum were grouped together.

Site-directed Mutagenesis—Polymerase chain reaction-based mutagenesis of the *T. brucei* γ-GCS expression vector was performed using the QuickChange™ site-directed mutagenesis kit from Stratagene as recommended by the manufacturer. 5′-3′ primers used to direct mutagenesis of the exact complement of the 6 metal-binding residues are listed as follows (the primers of other mutants that are not discussed in detail are not shown), with the replaced codon underlined. E53A, 5′-CCGTTTCTATGGGGAGACGCAATTGAACACCAGCTCGTCCGC-3′; E55A, 5′-GGGGAGACGAAATTGCACACCAGCTCGTCCGC-3′; E93A, 5′-GCAGAATGGCGCCCAGCATATGGGAGTTTTATGG-3′; E100A, 5′-GGGAGTTTTATGGTCGCGAGCCTCCCCGGCAAGCC-3′; E489A, 5′-GGGTGGCGTGTGGCGTTTCGTGTAATGGACG-3′; Q321A, 5′-GGGCTGCAACTGCCTTGCGCTTACCATGCAGCTTCCC-3′. All DNA encoding mutant enzyme were fully sequenced in their coding regions to verify the construct.

Protein Expression and Purification—T. brucei γ-GCS was expressed as a C-terminal His_8-tag fusion in a T7 bacterial (BL21/DE3 cells co-transformed with pREP4) expression vector. Protein was purified over a Ni^{2+}-agarose column followed by gel filtration (22). Protein solutions were stored in 50 mM Tris, pH 8, 100 mM NaCl, 5 mM $MgCl_2$ at 4 °C. Protein concentration was determined by absorbance at 280 nm with previously determined extinction coefficient (22).

Enzyme Kinetics Analysis of the γ-GCS Reaction by Spectrophotometric Assay—Kinetic analysis was done on purified γ-GCS at 37 °C with a spectrophotometric assay that couples ADP production with NADH oxidation (21). Buffer (100 mM Tris, pH 8.0, 150 mM NaCl, 2 mM phosphoenolpyruvate, 0.27 mM NADH) was mixed with 10 units/ml type III rabbit muscle pyruvate kinase, 20 units/ml of type II rabbit muscle lactic acid dehydrogenase, 5–60 mM total $MgCl_2$, and γ-GCS substrates. Unless otherwise stated, the following concentrations were used: 5 mM ATP, 100 mM L-Aba, and 10 mM L-Glu. L-Aba was substi-

FIG. 2. **Multiple sequence alignment for representative sequences of the γ-GCS and GS superfamily.** γ-GCS family sequences are *above* the *red line*. *E-I* represents animal/fungi sequences; *E-II* represents plant sequences. *P-I, P-II*, and *P-III* are prokaryotic groups. Three types of GSs (GS-I, -II, and -III) are shown *below* the *red line*. Each sequence is identified by the NCBI gene identification number (gi) except for those from the ERGO data base, which use the identifiers (*italicized*) in the ERGO data base. Sequence identifiers are followed by abbreviations of the species names. The archaeal and eukaryotic identifiers are marked with *red* and *green,* respectively, and the gi number of the sequence with known structure is *underlined* (gi|9256961, Protein Data Bank entry 1F52). The identifier of GS closest to the γ-GCS family members is shown in *bold* (gi|7478087). The first and the last residue numbers of the shown sequences are indicated, and the total length of the proteins is shown at the end (in *italicized numbers*). Only conserved motifs are shown. Residues in between the motifs are not displayed and the number of omitted residues is shown in *parentheses*. Uncharged residues at mainly hydrophobic positions are *shaded yellow*. Conserved small residues are in *blue bold letters*. The secondary structural elements are shown at the *bottom* according to the structure of *S. typhimurium* GS (PDB entry 1F52). β-Strands and α-helices are shown as *black arrows* and *green rectangles*, respectively. Conserved residues discussed in the text are marked by *numbers* (based on the *S. typhimurium* sequence) in the *boxes above* the GS sequences and those depicted on the structure diagram (Fig. 3) are shown in *white bold letters* on *black background*. The species name abbreviations are: *Aa*, *Actinobacillus actinomycetemcomitans*; *Af*, *A. fulgidus*; Ath, *Arabidopsis, thiliana*; *Ba*, *Buchnera aphidicola*; *Bf*, *Bacteroides fragilis*; *Bj*, *Brassica juncea*; *Ce*, *Caenorhabditis elegans*; *Dm*, *Drosophila melanogaster*; *Dr*, *Deinococcus radiodurans*; *Ec*, *E. coli*; *Efm*, *Enterococcus faecium*; *Efs*, *Enterococcus faecalis*; *Hsp*, *Halobacterium* sp.; *Mt*, *Mycobacterium tuberculosis*; *Mtr*, *Medicago truncatula*; *Pa*, *Pseudomonas aeruginosa*; *Pm*, *Pasteurella multocida*; *Psp*, *Pseudomonas* sp.; *Sc*, *Streptomyces coelicolor*; *Sce*, *S. cerevisiae*; *Sm*, *Streptococcus mutans*; *Ssp*, *Synechocystis sp.*; *St*, *Salmonella typhimurium*; *Tb*, *T. brucei*; *Vc*, *Vibrio cholerae*; *Xf*, *Xylella fastidiosa*; *Yp*, *Yersinia pestis*; *Zm*, *Zymomonas mobilis.*

tuted for L-Cys in all kinetic studies. Previous studies used KCl instead of NaCl but we found KCl to be inhibitory at high concentrations. The reaction was begun with the addition of γ-GCS. Enzyme concentration ranges were as follows: wild-type γ-GCS, 0.1–0.4 μM; E489A and Q321A, 30–60 μM with Mg^{2+} and 0.4–1.4 μM with Mn^{2+}; E53A, E55A, E93A, and E100A, 4–30 μM. For the metal binding studies, the protein samples (10–20 ml) were dialyzed twice against 4 liters of buffer without divalent metals. Divalent metal in the form of $MgCl_2$ or $MnCl_2$ was added to the reaction over a range of free concentrations. The concentration of free metal was determined at a given total metal concentration and ATP concentration under the conditions of the assay with the program "Bound and Determined" (28). When using Mn^{2+}, the above reaction buffer was modified to use 15 units/ml of type III rabbit muscle pyruvate kinase and 30 units/ml of type II rabbit muscle lactic acid dehydrogenase. Reaction rates were confirmed to be linear with enzyme concentration. All curve fitting and modeling of kinetic data was performed using Sigma Plot 5.0 (SPSS Inc.).

HPLC Analysis of Product Formation—E93A γ-GCS was incubated with L-Glu (10 mM for wild-type γ-GCS and 100 mM for E93A), L-Aba (20 mM), and ATP (5 mM) in buffer (40 mM MOPS, pH 8.0, 20 mM NaCl, and 5 mM $MgCl_2$) at 37 °C for 30 min. The reactions were stopped with the addition of trichloroacetic acid (final concentration of 7%). L-Aspartate (final concentration of 7.7 mM) was added as an internal standard. Aliquots of the samples were derivatized using the AccQ_TAG kit (Waters, Milford, MA) with certain changes. Derivatization (125 μl total volume) took place in buffer (170 mM MOPS, pH 8.0, 1.4 mM EDTA) using 25 μl of the enzyme reaction and 31 μl of the AccQ_TAG kit reagent at 55 °C for 10 min. Sample (7 μl) was injected onto an AccQ_TAG column using published buffers and gradient (29). A Beckman System Gold™ HPLC was used and peaks were monitored at 248 nm. The column was calibrated using standard samples of the following compounds, derivatized as above: L-Asp (RT = 17.1 min), L-Glu (RT = 19.7 min), L-Aba (RT = 28.6 min), and γ-glutamylaminobutryate (RT = 25.1 min). The concentration of dipeptide product in the analyzed samples was determined from a standard curve generated from known concentrations of the compounds with respect to the internal standard.

RESULTS

Identification of Homology among γ-GCS Proteins

To clarify the relationships among γ-GCS proteins from different organisms, we conducted PSI-BLAST searches starting from individual sequences from fungi, plants, and bacteria. Similarity searches initiated with plant sequences retrieved a hypothetical protein from *Synechosytis* sp. (gi|7469602, iteration 2, E-value 0.05). Using this protein as the query we detected many bacterial sequences as well as sequences from plants (*e.g.* gi|7489004, *L. esculentum*, iteration 3, E-value 4e-05), animals (*e.g.* gi|7494173, *Plasmodium falciparum*, iteration 3, E-value 0.044), and fungi (*e.g.* gi|885591, *Schizosaccharomyces pombe*, iteration 4, E-value 0.007), implying that these γ-GCSs are homologous. Searches with the *E. coli* γ-GCS sequence (gi|121661) converged within a separate bacterial group that could not be linked with other γ-GCSs using PSI-BLAST. However, analysis of conserved motifs and secondary structure

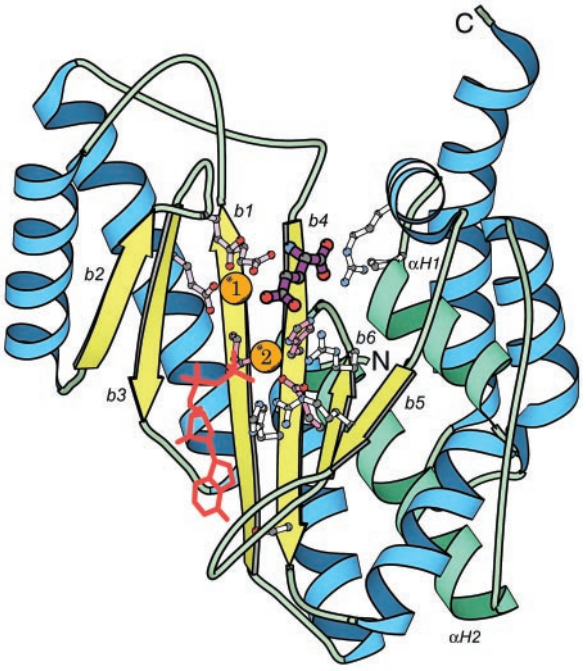

FIG. 3. **Structure of the C-terminal domain of type I GS.** The structure of the C-terminal domain of *S. typhimurium* GS is displayed (Protein Data Bank entry 1F52, chain A, residues 102–462). Secondary structure elements are labeled by *italicized letters* and *numbers*. β-Strands and hydrophobic α-helices and are labeled with *b* and *αH*, respectively, followed by the corresponding number. The two hydrophobic helices are shown in *green*. Conserved residues are shown in ball-and-stick representations. The two metal ions n1 and n2 are shown as *orange balls*. Side chains of n1 and n2 metal-binding residues are shaded in *light purple* and *pink*, respectively. ADP is displayed in *red lines*; L-Glu is in *magenta* using the ball-and-stick representation. The figure was drawn with the program BOBSCRIPT (43).

predictions in this group, and their comparison with other γ-GCSs, suggested homology among all known γ-GCS proteins (Fig. 2). Based on sequence similarities and phylogeny of organisms, we divided γ-GCS homologues into two eukaryotic groups (E-I and E-II) and three prokaryotic groups (P-I, P-II, and P-III) (Fig. 2).

Identification of GS as a Structural Homolog of γ-GCS

PSI-BLAST searches starting from γ-GCS sequences could not detect any proteins outside the γ-GCS family with significant E-values (<0.02). Because the sensitivity of profile-based similarity searches relies on the quality of the multiple sequence alignment, alignments produced automatically by PSI-BLAST might be of insufficient quality to detect remote homologues. Thus after automated PSI-BLAST iterations failed to detect γ-GCS homologues with statistically significant scores, we used the manually adjusted multiple alignment of all identified γ-GCS sequences to start profile-based searches. For some query sequences (for example, gi|11282603 from *Xylella fastidiosa*, Fig. 2), seeding PSI-BLAST with the γ-GCS alignment produced significant hits (E-value less than 0.02, bit score >40) to a protein outside the γ-GCS family. This *Mycobacterium tuberculosis* protein (gi|7478087) is annotated as "probable glnA3 protein" and belongs to the type I GS family (Fig. 2). No other proteins were detected with E-values less than 0.02. The key residues for metal and substrate binding or catalysis in GS form highly conserved motifs that are mainly located in the central β-sheet (Fig. 3). An inspection of the multiple sequence alignments of γ-GCS and GS reveals consistent conservation of these key residues (Fig. 2). Additionally, hydrophilic and hydrophobic positions alternate along the predicted β-strands, and secondary structure prediction (27) of the aligned regions are similar (data not shown). Thus we conclude that γ-GCSs and GSs are homologous and unify them into a superfamily of carboxylate-amine/ammonia ligases.

Structural Features of the GS / γ-GCS Superfamily

The GS from *Salmonella typhimurium* has been thoroughly studied and its structure has been determined (19, 20). Only the C-terminal domain of GS is homologous to γ-GCS and it consists of a central anti-parallel β-sheet of 6 strands with several α-helices packed on one side of it (Fig. 3). The other side of the β-sheet accommodates the active site with the binding sites for metal ions and substrates. All of the core β-strands and α-helices of GS can be mapped to the γ-GCS sequences, among which are two hydrophobic α-helices buried between the β-sheet and outside helices (Fig. 2). Two divalent metal ions (termed n1 and n2, which may be Mg^{2+} or Mn^{2+}) participate in substrate binding and catalysis by GS. The n1 metal interacts with the α-carboxyl group of L-Glu and the n2 metal interacts with ATP and is involved in phosphoryl transfer. Each metal is chelated by three highly conserved residues: the n1 metal is liganded by Glu-131, Glu-212, and Glu-220 and the n2 metal is bound by Glu-129, His-269, and Glu-357 (Fig. 3). Five of the metal ligands are conserved throughout the γ-GCS and GS families, while His-269 is conservatively replaced with Gln in many γ-GCS proteins (Fig. 2). The conservation of metal-binding residues across the superfamily suggests that γ-GCS also binds two metal ions that are chelated similarly. The binding sites for L-Glu and ATP are also predicted to be similar between GS and γ-GCS, while the third substrate differs between the two (ammonia in GS *versus* L-Cys in γ-GCS) and the binding pockets are not expected to be conserved. The negative charges of the ATP phosphoryl groups in GS are mainly stabilized by the n2 metal and by Arg-344, which is conserved in both families (Fig. 2). His-271 also interacts with the phosphates of ATP in GS and is replaced by Asn or Thr in many of the γ-GCS sequences, while Ser-273, which forms a hydrogen bond to N-6 of the ATP purine ring in GS is replaced by Ser, Asp, or Gln in γ-GCS (Fig. 2). In GS two arginine residues confer the substrate specificity for L-Glu, Arg-321 interacts with the α-carboxyl and Arg-359 with the γ-carboxylate of L-Glu (Figs. 2 and 3). The corresponding positions in γ-GCS also contain a positively charged residue (typically Arg), suggesting that L-Glu binds to γ-GCS in a similar manner.

Diversity of γ-GCS and GS Superfamily

The difficulty in identifying the relationship between the γ-GCS and GS families results from the fact that this superfamily of carboxylate-amine/ammonia ligases is very diverse, *e.g.* with sequence identity ranging from 7 to 92% for the full-length sequences in Fig. 2. Thus, it is not straightforward to build a phylogenetic tree for the superfamily, the branching order in such a tree would be highly unreliable. To illustrate the relationships between the superfamily members, we have chosen to represent the sequences as points in Euclidian space with distances between the points approximating evolutionary distances. The two-dimensional projection of the space onto the plane of the largest scatter of points is shown (Fig. 4). The points were grouped according to the procedure described under "Experimental Procedures" resulting in 7 clusters that are colored differently on the distance projection plot (Fig. 4). Sequences that are more closely related group together on the plot. Eukaryotic group I (E-I) contains animal and fungal sequences; they share high sequence similarities. E-II/P-I consists of plant and prokaryotic sequences, which are similar to each other and relatively distant from animal or fungal sequences. The high similarity between plant and prokaryotic

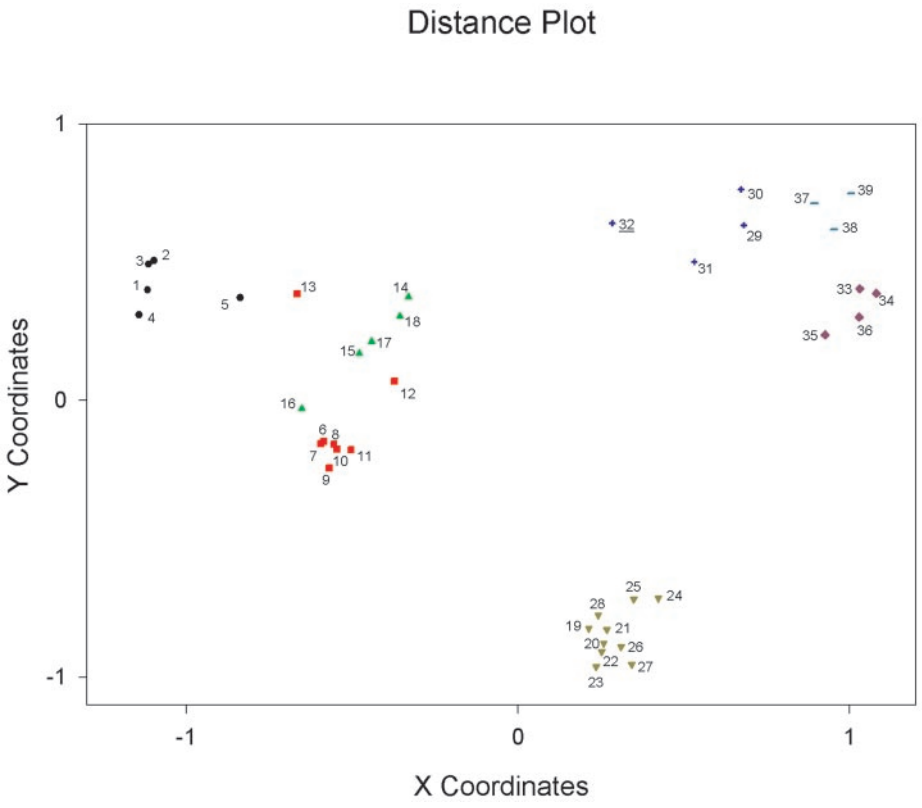

FIG. 4. **Distance diagram of representative sequences of γ-GCS and GS.** Coordinates 1 and 2 are the two dimensions of maximal scatter of points in a multidimensional space. The points represent the sequences in Fig. 2, numbered correspondingly. The representations are: *filled black circles* (E-I, 1–5), *red rectangles* (E-II/P-I, 6–13), *green triangles* (P-II, 14–18), *dark yellow-green triangles* (P-III, 19–28), *purple plus signs* (GS-I, 29–32), *brown diamonds* (GS-II, 33–36), and *cyan lines* (GS-III, 37–39). The PSI-BLAST link sequence (number 32, gi|7478087) between γ-GCS and GS is *underlined*.

sequences from this group might suggest horizontal transfer events between plants and bacteria/archaea. The distance plot shows that sequences of groups E-II/P-I and P-II are closer to each other than to any other group. In contrast, the P-III group is well separated from the rest and it includes the first experimentally characterized prokaryotic γ-GCS from *E. coli* (30). Finally, the GS sequences, which have been classified into three groups, are distant from all of the γ-GCS sequences and group together on the plot.

The sequences in the P-II group and many prokaryotic sequences in the E-II/P-I group are hypothetical proteins without functional annotations. Their detected homology to γ-GCS facilitates functional annotation and classification of these sequences. Two archaeal proteins (gi|11499888 from *Archaeoglobus fulgidus* and gi|10580902 from *Halobacterium sp.*) are among these hypothetical proteins. There have been no previous reports about the presence of γ-GCS in archaea. Our detection of γ-GCS in *Halobacterium sp.* is consistent with previous findings that γ-glutamylcysteine dipeptide is one of the major thiols in halobacteria in the absence of significant glutathione (31).

Characterization of Metal Dependence by Wild-type T. brucei γ-GCS

The finding that γ-GCS is a structural homolog of GS supports the conclusion that γ-GCS has two metal-binding sites. To evaluate this hypothesis experimentally, the dependence of the reaction rate of wild-type γ-GCS on free Mg^{2+} was monitored. The concentrations of free metal and MgATP were calculated from total metal and ATP concentrations by using the computer program "Bound and Determined" (28). Saturating concentrations of MgATP, L-Glu, and L-Aba were used for the analysis. A hyperbolic dependence of the reaction rate on free Mg^{2+} was observed (Fig. 5). The data were fitted to the Michaelis-Menten equation and the K_d^{app} (apparent dissociation constant) for free Mg^{2+} at 2 mM ATP was determined to be 0.50 ± 0.04 mM (Table I). Small variations in the concentration of MgATP (less than a 2-fold change occurs over the 35-fold range of free Mg^{2+}) did occur over the range of the titration but were not substantial enough to account for the rate activation by free Mg^{2+}. Thus, the data are consistent with the model derived from the GS structure in which the active enzyme species binds both Mg^{2+} and MgATP at separate sites.

Effects of Substituting Mn^{2+} for Mg^{2+}

Wild-type *T. brucei* γ-GCS is also activated by Mn^{2+} (Fig. 5). The activity is stimulated at significantly lower concentrations of Mn^{2+} (EC_{50} = 6 μM) than Mg^{2+}, however, the maximum catalytic rate is slightly lower. Total Mn^{2+} concentrations above 0.75 mM are inhibitory. Unlike for Mg^{2+}, the dependence of rate on free Mn^{2+} concentrations is sigmoidal and suggests multiple Mn^{2+} ions may be binding cooperatively. Indeed the concentration of MnATP could not be held constant over the range of free Mn^{2+} concentrations used in the titration, thus the data reflect contributions from the binding of both free Mn^{2+} and MnATP to separate sites on the enzyme.

The kinetic constants for all three substrates were also measured in the presence of constant concentration of free Mn^{2+}. The K_m values for L-Glu and Aba were similar to those measured in the presence of Mg^{2+} and the K_m for MnATP was 3-fold lower than for MgATP (Tables II and III).

Steady-state Kinetic Analysis

Mutation of n1 Metal-binding Residues—Based on the multiple sequence alignment of GS with γ-GCS family members, residues Glu-55, Glu-93, and Glu-100 of *T. brucei* γ-GCS were identified as the n1 metal ligands and would be expected to form the free Mg^{2+}-binding site (Fig. 2). Mutation of these residues to Ala drastically reduced k_{cat} (Table II). The activities of the E55A and E100A mutants were not distinguishable from background rates in the presence of either Mg^{2+} or Mn^{2+}. The k_{cat} of E93A (k_{cat} = 0.066 ± 0.005 s^{-1}) is 60-fold lower than for wild-type γ-GCS based on the coupled spectrophotometric assay that follows ATP hydrolysis to ADP. Moreover, the K_m^{app} for L-Glu rises 46-fold to

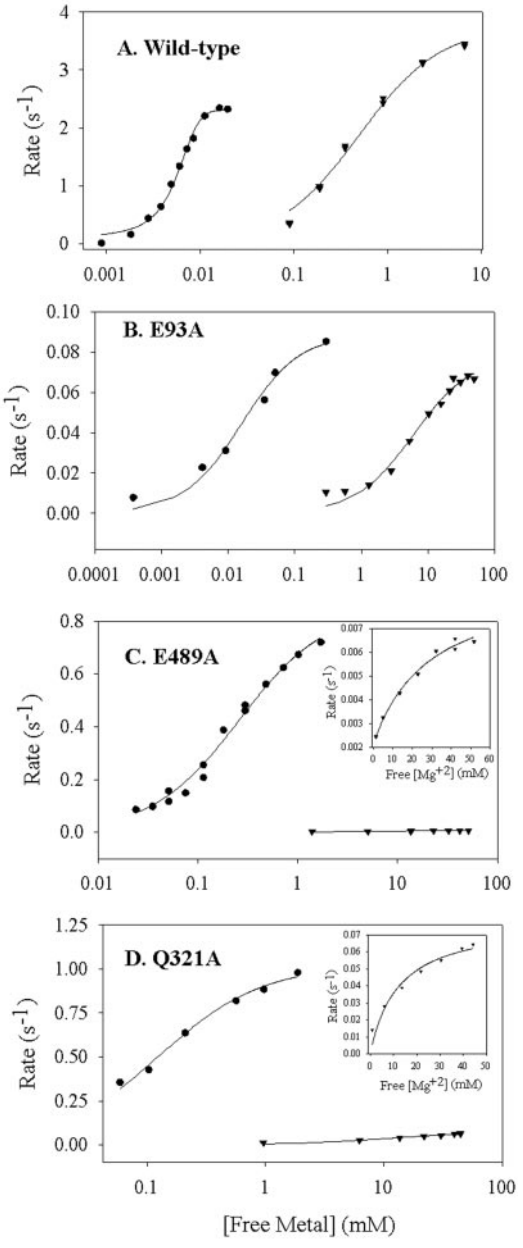

FIG. 5. **Divalent metal activation of wild-type and mutant γ-GCS.** The dependence of enzyme rate on free Mn^{2+}(●) or Mg^{2+} (▼). Free metal concentration was calculated from total metal concentration using the program "Bound and Determined." *Lines* represent the fit of the displayed data to the Michaelis-Menten equation. The concentrations for L-Glu and L-Aba in all experiments were 10 and 100 mM, respectively. The concentrations of ATP in the assays were: *A,* wild-type, 2 mM; *B,* E93A, 5 mM; *C,* E489A, 5 mM; and *D,* Q321A, 15 mM. Wild-type data with Mn^{2+} was fit to the Hill equation ($n = 2.5$) as a hyperbola did not fit the data (see "Results"). The square of the correlation coefficient (r^2) for the global fit of all displayed data are greater than 0.98. For *panels C* and *D*, the *insets* show an expanded view of the hyperbolic enzyme rate dependence on free Mg^{2+} concentration.

11 ± 2 mM, consistent with the proposed role for the n1 metal in L-Glu binding. The rate of ATP hydrolysis catalyzed by E93A γ-GCS is activated by free Mg^{2+} but requires 12-fold higher concentrations (K_d^{app} = 6.1 ± 0.9 mM; Table I) than for the wild-type enzyme to achieve the maximal rate under saturating substrate conditions (Fig. 5). The concentration of MgATP was held constant over the range of Mg^{2+} concentrations tested, supporting the conclusion that the titration represents Mg^{2+} binding to the n1 site. E93A γ-GCS is also activated by free Mn^{2+} (K_d^{app} = 16 ± 3 μM) at similar concentrations to the wild-type enzyme. The dependence of the reaction rate on free Mn^{2+} concentration is hyperbolic suggesting that only a single site is involved in the titration. However, this titration may represent interactions at the n2 site and not the n1 site, since the concentration of MnATP also varies during the titration.

Interestingly, while the reaction catalyzed by E93A is L-Glu dependent, it is not dependent on L-Aba over a concentration range from 0 to 200 mM. Analysis of this reaction by HPLC shows that the dipeptide product, γ-glutamylaminobutyrate, was not formed during the course of the reaction catalyzed by the E93A enzyme (Fig. 6). In contrast for the wild-type enzyme, the rate of formation of γ-glutamylaminobutyrate determined by HPLC analysis exactly corresponds to the rate of ADP formation measured in the spectrophotometric assay. These data demonstrate that the mutant enzyme is capable of hydrolyzing ATP in a L-Glu-dependent reaction but cannot catalyze the peptide bond ligation between L-Glu and L-Aba.

Mutation of n2 Metal-binding Residues—The n2 metal-binding residues of GS align with residues Glu-53, Gln-321, and Glu-489 of *T. brucei* γ-GCS (Fig. 2). Mutation of these residues to Ala dramatically lowers the reaction rate catalyzed by the enzyme (Table II). E53A γ-GCS has no detectable activity, consistent with a role for this residue as a crucial ligand for the n2 metal site. The k_{cat} of the E489A enzyme falls 720-fold to 0.0053 ± 0.0005 s^{-1}. In addition, the K_m^{app} for ATP rises 28-fold while negligible effects were observed on the other two substrates. The effects of mutating Gln-321 to Ala are focused on MgATP binding. The enzyme rate does not saturate with increasing MgATP concentrations up to the limit of the assay ([ATP] = 15 mM) and the k_{cat}/K_m^{app} for MgATP is 3.7 ± 0.4 M^{-1} s^{-1}, a 14,000-fold decrease compared with the wild-type enzyme. The K_m^{app} values for the other two substrates were not changed, although it is important to note that these data could not be obtained at saturating MgATP levels. The kinetic analysis of E53A, E489A, and Q321A γ-GCS points to their role in binding the n2 metal and are consistent with the observation in GS that the n2 metal ion coordinates the γ-phosphate oxygen of ATP to allow phosphoryl transfer in the first step of the reaction (20, 32).

Higher concentrations of free Mg^{2+} are required for full activation of both the E489A (36-fold) and Q321A (26-fold) mutant enzymes (Table I, Fig. 5). The concentration of MgATP does not vary over the course of the titration and, similar to wild-type γ-GCS, the measured apparent K_d values most likely reflect binding of free Mg^{2+} to the n1 site. Thus, these data do not provide direct information about the interaction of MgATP at the mutated n2 site. Rather, the data suggest that the n2 and n1 sites either interact cooperatively or that if Mg and MgATP bind in an ordered mechanism, that mutation of the n2 site effects the apparent K_d^{Mg} by shifting the equilibrium.

Surprisingly, substitution of Mn^{2+} for Mg^{2+} in the enzyme assay rescued the activity of the E489A and Q321A mutant enzymes. In the presence of Mn^{2+}, nearly wild-type γ-GCS rates were observed with both the E489A and Q321A mutant enzymes (Table I, Fig. 5). Similarly to the wild-type enzyme, significantly lower concentrations of Mn^{2+} are required for full enzyme activation compared with Mg^{2+} and again the titration represents the effects of changes in both free Mn^{2+} and MnATP. However, higher concentrations of Mn^{2+} (20–50-fold) are required to activate the mutant enzymes compared with wild-type γ-GCS and this result is at least in part likely to be a reflection of changes in binding of MnATP to the n2 site. For the E489A mutant the activation of the enzyme by Mn^{2+} is largely a k_{cat} effect, as the K_m for MnATP is as significantly changed from that observed for MgATP (Table III). The K_m values for the other two substrates, L-Glu and Aba, do not differ

TABLE I
Metal activation of T. brucei γ-GCS mutants

Values were obtained by fitting rate data to the Michaelis-Menten equation. Errors are the standard error of the fit. Data were collected with the following substrate concentrations: 10 mM L-Glu; 100 mM L-Aba; and 2, 5, and 15 mM ATP in wild-type, E489A, and Q321A γ-GCS, respectively.

Enzyme	k_{cat} Mg^{2+}	K_d^{app} Mg^{2+}	k_{cat} Mn^{2+}	K_d^{app} Mn^{2+}
	s^{-1}	mM	s^{-1}	mM
Wild-type	3.8 ± 0.1	0.50 ± 0.04	2.5[a]	0.006[a]
E93A	0.078 ± 0.003	6.1 ± 0.9	0.089 ± 0.005	0.016 ± 0.003
E489A	0.0066 ± 0.0005	18 ± 4	0.89 ± 0.03	0.28 ± 0.02
Q321A[b]	0.08	13 ± 4	1.5 ± 0.0	0.13 ± 0.01

[a] The Mn^{2+} dependence of wild-type γ-GCS was sigmoidal and this value represents an EC_{50}.
[b] The rate for the Q321A mutant did not saturate with Mg^{2+} ATP concentration. k_{cat} Mg^{2+} is the highest observed rate at saturating metal concentration and fixed substrate concentrations.

TABLE II
Kinetic analysis of T. brucei γ-GCS mutants in the presence of Mg^{2+}

k_{cat} and K_m, app values were obtained by fitting the rate data to the Michaelis-Menten equation. Errors are the standard error of the fit. Errors are not reported for k_{cat}/K_m^{app} except when the ratio was calculated experimentally. The reported k_{cat} is the fitted parameter obtained from varying ATP over its dynamic concentration range. The fixed substrate concentrations were: L-Glu (10 mM), L-Aba (100 mM), and ATP (5 mM), with the following exceptions: for E93 L-Glu was 100 mM and for Q321A ATP was 15 mM. The total $MgCl_2$ concentrations were: 50 mM in the E53A, E55A, E93A, E100A, and E489A mutant enzymes; 20 mM for the wild-type enzyme, and 60 mM in the Q321A enzyme. Under these conditions, all ATP in the assay is present as MgATP.

Enzyme	k_{cat} (MgATP)	K_m^{app} L-Glu	K_m^{app} L-Aba	K_m^{app} MgATP	k_{cat}/K_m^{MgATP}
	s^{-1}		mM		M^{-1} s^{-1}
Wild-type[a]	3.8 ± 0.1	0.24 ± 0.02	10 ± 1	0.071 ± 0.010	53,000
E55A[b]	ND				
E93A	0.066 ± 0.005	11 ± 2	N.D.[c]	0.32 ± 0.08	210
E100A[b]	ND				
E53A[b]	ND				
Q321A[d]	>0.24	1.6 ± 0.3	18 ± 3	>45	3.7 ± 0.4
E489A[e]	0.0053 ± 0.0005	1.1 ± 0.1	15 ± 2	2.0 ± 0.5	2.7

[a] k_{cat} is the fitted parameter from varying Mg^{2+} over its dynamic concentration range. The error is the standard error of the fit to the Michaelis-Menten equation. This value is in agreement with previously reported k_{cat} (22). K_m^{app} values for wild-type γ-GCS were taken from Ref. 21.
[b] These three mutant enzymes had no detectable (N.D.) activity above background (determined by rate of reaction without L-Glu) and the rates are at least 10^3-fold lower rate than wild-type γ-GCS k_{cat} under the following assay conditions (L-Aba, 100 mM; L-Glu, 10 mM; ATP, 5 mM; total $MgCl_2$, 50 mM).
[c] N.D., not detected. This mutant displayed no rate dependence on L-Aba concentration (0–200 mM).
[d] The rate for this mutant had a linear dependence on ATP concentration over the tested range (0–15 mM). K_m^{app} values for L-Glu and L-Aba were measured at 15 mM ATP. Minimum values for k_{cat} and K_m^{app} for ATP were estimated by assuming the K_m^{app} for ATP is at least 3-fold higher than the highest tested concentration.
[e] The E489A mutant had significant background activity in the presence of Mg^{2+} (determined by the rate of the reaction without L-Glu) and the background rate was subtracted from the rate data for analysis.

TABLE III
Kinetic analysis of T. brucei γ-GCS n2 metal binding mutants in the presence of Mn^{2+}

Enzyme	k_{cat} (MnATP)	K_m^{app} L-Glu	K_m^{app} L-Aba	K_m^{app} MnATP	k_{cat}/K_m^{MnATP}
	s^{-1}		mM		M^{-1} s^{-1}
Wild-type[a]	2.4 ± 0.0	1.0 ± 0.0	6.0 ± 0.5	0.022 ± 0.001	110,000
E489A	0.89 ± 0.03	0.65 ± 0.01	9.4 ± 0.7	0.1 ± 0.0	8,100
Q321A	1.5 ± 0.0	1.1 ± 0.1	14 ± 2	1.2 ± 0.1	1,300

[a] k_{cat} and K_m^{app} values were obtained by fitting the rate data to the Michaelis-Menten equation. Errors are the standard error of the fit. The reported k_{cat} is the fitted parameter obtained from varying MnATP over its dynamic concentration range. One substrate was varied over a concentration range above and below K_m while the other substrates were present at fixed concentration. The fixed substrate concentrations were: L-Glu (10 mM), L-Aba (100 M), and ATP (1 mM for wild-type enzyme and 5 mM for E489A and Q321A mutant enzymes). Free Mn^{2+} concentrations were kept constant in all experiments at: 0.025 mM in wild-type enzyme; 1.7 mM in the E489A γ-GCS, and 2 mM in the Q321A enzyme.

if the activating metal is Mg^{2+} or Mn^{2+}. In contrast, for the Q321A mutant, the K_m for MnATP is significantly lower than for MgATP and the activation of the enzyme by Mn^{2+} results from the lowering of the K_m for this substrate. The K_m for MnATP is, however, 55-fold higher than for the wild-type enzyme. The K_m values for L-Glu and Aba are similar in the presence of Mn^{2+} or Mg^{2+}.

DISCUSSION

The data presented in this paper provides the first important insight into the three-dimensional structure of γ-GCS and into the composition of the enzyme active site. The structural prediction that γ-GCS is a homolog of the well characterized enzyme GS opens the way for detailed mechanistic analysis of the enzyme to understand the roles of active site residues in catalysis. The GS/γ-GCS superfamily is composed of a diverse set of sequences that made identification of the homology between the family members difficult. However, the evidence for this homology is clear and compelling. PSI-BLAST analysis using optimized sequence alignments identified the connection between the families. The secondary structural elements determined for the GS structure are predicted to be conserved in the γ-GCS family members and the key residues for metal and substrate binding or catalysis identified in GS, form motifs that are highly conserved throughout the entire GS/γ-GCS superfamily. Finally, we have confirmed that the residues predicted to form the two metal-binding sites in γ-GCS play analogous roles in catalysis and substrate binding to those described for GS.

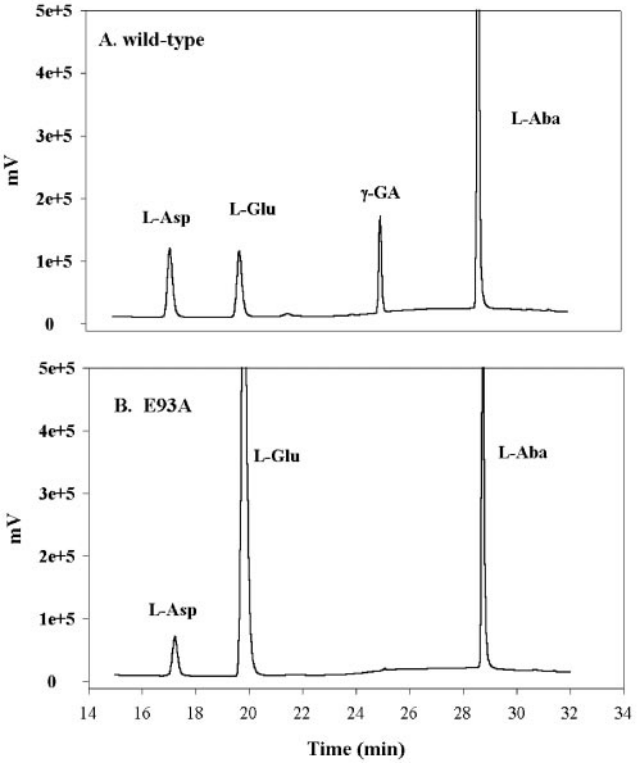

FIG. 6. **Product formation in wild-type and E93A *T. brucei* γ-GCS.** Results from HPLC analysis of reaction products in wild-type and E93A γ-GCS. Representative samples are displayed where reactions were incubated for 30 min at 37 °C in a modified MOPS buffer in the presence of 5 mM ATP, 20 mM L-Aba. (*A*) 10 mM L-Glu and 2.6 μM wild-type γGCS. *B*, 100 mM L-Glu and 125 μM E93A γ-GCS. Retention times were used to identify peaks, which are labeled on the chromatogram (plot of mV recorded on the detector *versus* retention time). γGA, γ-glutamylaminobutyrate.

Based on homology to GS, γ-GCS is predicted to bind two metal ions that are essential for catalysis. The rate of the reaction catalyzed by the wild-type enzyme has a hyperbolic dependence on the concentration of free Mg^{2+}. Since the concentration of MgATP does not change significantly during the titration, these data support the structural prediction that γ-GCS binds two metals, one as Mg^{2+} and one as MgATP. Furthermore, Mn^{2+} also activates the enzyme; however, the rate dependence on Mn^{2+} concentration is likely a reflection of the binding of both free Mn^{2+} and MnATP. Similar results were observed for the activation of GS with both Mg^{2+} and Mn^{2+} (33).

The metal ions are each chelated by three amino acid residues that compose the core of the active site of γ-GCS: n1 liganded by Glu-55, Glu-93, and Glu-100, and n2 liganded by Glu-53, Gln-321, and Glu-489. Of these six residues, five are invariant between the γ-GCS and GS families. The n1 metal ligands Glu-55, Glu-93, and Glu-100 bind the free metal that interacts with L-Glu during the reaction. Mutation of all three residues to Ala had a dramatic impact on catalytic function. Two mutant enzymes, E55A and E100A, retained no detectable activity. The third, E93A γ-GCS is only capable of catalyzing L-Glu-dependent ATP hydrolysis and not the ligation reaction between L-Glu and L-Aba. The apparent K_d for interaction with free Mg^{2+} increases by 12-fold and the specificity constant for L-Glu (k_{cat}/K_m^{app} for L-Glu) in this partial reaction is diminished 2600-fold from the wild-type enzyme value. These data suggest a role for the n1 metal in interacting with the γ-carboxylate of L-Glu and in stabilizing the transition state formed during attack of the L-Aba α-amino group on the γ-phosphorylated L-Glu intermediate. While the analogous mutations have not been reported in GS, the n1 metal-binding site has been shown by kinetics and spectral changes to be crucial for enzyme stability (34). Furthermore, equilibrium binding studies and kinetic analysis of GS (35), as well as x-ray crystallographic studies (20), demonstrate that the n1 metal is an L-Glu binding determinant in GS. These results support our conclusion that the n1 metal-binding site in γ-GCS plays an important role in L-Glu binding and in transition state stabilization leading to the formation of the dipeptide product.

The n2 metal-binding site in γ-GCS, composed of residues Glu-53, Glu-489, and Gln-321, binds and positions MgATP for the reaction. Mutation of all three residues to Ala significantly decreases the catalytic efficiency of the enzyme. Glu-53 is possibly the most crucial ligand for the n2 metal in γ-GCS since its mutation to Ala results in an enzyme with no detectable activity. Mutation of Glu-489 decreased k_{cat} substantially and increased the apparent K_m for MgATP. Mutation of Q321A had a particularly large effect on the apparent K_m for MgATP as saturation of the enzyme by MgATP could not be observed. These data suggest that Glu-489 and Gln-321 are important for positioning the n2 metal to promote MgATP binding and subsequent phosphoryl transfer. A role for metals in correctly positioning reaction components for phosphoryl transfer has been observed in model compound studies (36). The data are consistent with studies in GS where the n2 metal plays a role in ATP binding, as evidenced by equilibrium binding and kinetic studies (32). Mutation of residues analogous to Glu-53 and Glu-489 in GS (Glu-129 and Glu-357) results in enzyme with very low catalytic activity (37). However, mutation of His-269 in GS did not significantly affect ATP binding (38), whereas the Q321A mutant dramatically affected K_m^{app} for ATP. These differences in functional roles may be partially explained by the different properties of metals liganded to nitrogen or oxygen. X-ray structures of proteins in which Gln is a metal ligand demonstrate that Gln typically binds divalent metal via the carbonyl oxygen (39).

Substitution of Mn^{2+} for Mg^{2+} rescued the activity deficits in E489A and Q321A γ-GCS. Unlike the effects of Mg^{2+} on the rate dependence of the reaction, the effects of Mn^{2+} may result from interactions at either or both of the two metal-binding sites, since the concentrations of both free Mn^{2+} and MnATP change during the titration of the metal. The Mn^{2+} activation of the E489A mutant enzyme is clearly a k_{cat} effect. In contrast, activation of Q321A γ-GCS by Mn^{2+} results from the fact that the K_m for MnATP is significantly lower than for MgATP. Differential effects on catalytic efficiency between Mn^{2+} and Mg^{2+} have also been described for the n2 metal ligand mutants in GS (37, 38) and for phosphodiesterase-5 (40). Mn^{2+} forms bidentate carboxylate complexes with ligands whereas Mg^{2+} cannot (41). In the mutant enzymes, Mn^{2+} may be able to take advantage of this type of interaction with one of the remaining carboxylate ligands to retain proper orientation for effective catalysis and substrate binding. Mg^{2+} and Mn^{2+} also differ in their diameter, polarizability, and average distance of the metal-oxygen bond (39, 41). These varied properties may produce changes in the orientation of the reacting substrates. Small perturbations that affect the overlap of the reacting orbitals in the transition state have been demonstrated to have large effects on catalysis (42).

In summary, these data are a strong first step in understanding the active site of γ-GCS. We have elucidated two metal-binding sites, termed n1 and n2, and identified their amino acid ligands. Furthermore, these studies provide insight into the roles of both metals and their ligands in substrate binding and catalysis of γ-GCS. However, other important residues

such as acid/base catalysts or those involved in substrate binding, especially L-Cys, remain to be defined.

Acknowledgments—We thank Dr. Joseph Albanesi and Dr. Elliot Ross for helpful discussions.

REFERENCES

1. Meister, A. (1989) *Metabolism and Function of Glutathione* (Avramovic, D., and Poulson, R., eds) Part A, pp. 367–474, John Wiley and Sons, Inc. New York
2. Hayes, J. D., and McLellan, L. I. (1999) *Free Radic. Res.* **31,** 273–300
3. Wang, C. C. (1995) *Annu. Rev. Pharmacol. Toxicol.* **35,** 93–127
4. Fairlamb, A. H., and Le Quesne, S. A,. (1997) *Trypanosomiasis and Leishmaniasis* (Hide, G., Mottram, J. C., Coombs, G. H., and Holmes, P. H., eds) pp. 149–161, CAB International, Wallingford, Oxen, UK
5. Griffith, O. W., and Mulcahy, R. T. (1999) *Adv. Enzymol. Relat. Areas Mol. Biol.* **73,** 209–267
6. Griffith, O. W. (1999) *Free Radic. Biol. Med.* **27,** 922–935
7. Grondin, K., Haimeur, A., Mukhopadhyay, R., Rosen, B. P., and Ouellette, M. (1997) *EMBO J.* **16,** 3057–3065
8. Orlowski, M., and Meister, A. (1971) *J. Biol. Chem.* **246,** 7095–7105
9. Orlowski, M., and Meister, A. (1971) *Biochemistry* **10,** 372–380
10. May, M. J., and Leaver, C. J. (1994) *Proc. Natl. Acad. Sci. U. S. A.* **91,** 10059–10063
11. Galperin, M. Y., and Koonin, E. V. (1997) *Protein Sci.* **6,** 2639–2643
12. Altschul, S. F., Madden, T. L., Schaffer, A. A., Zhang, J., Zhang, Z., Miller, W., and Lipman, D. J. (1997) *Nucleic Acids Res.* **25,** 3389–3402
13. Eddy, S. R. (1996) *Curr. Opin. Struct. Biol.* **6,** 361–365
14. Aravind, L., and Koonin, E. V. (1999) *J. Mol. Biol.* **287,** 1023–1040
15. Gribskov, M., McLachlan, A. D., and Eisenberg, D. (1987) *Proc. Natl. Acad. Sci. U. S. A.* **84,** 4355–4358
16. Henikoff, J. G., and Henikoff, S. (1996) *Comput. Appl. Biosci.* **12,** 135–143
17. Eddy, S. R. (1998) *Bioinformatics* **14,** 755–763
18. Ginsburg, A. (1972) *Adv. Protein Chem.* **26,** 1–79
19. Eisenberg, D., Gill, H. S., Pfluegl, G. M., and Rotstein, S. H. (2000) *Biochim. Biophys. Acta* **1477,** 122–145
20. Liaw, S. H., and Eisenberg, D. (1994) *Biochemistry* **33,** 675–681
21. Lueder, D. V., and Phillips, M. A. (1996) *J. Biol. Chem.* **271,** 17485–17490
22. Brekken, D. L., and Phillips, M. A. (1998) *J. Biol. Chem.* **273,** 26317–26322
23. Henikoff, S., and Henikoff, J. G. (1992) *Proc. Natl. Acad. Sci. U. S. A.* **89,** 10915–10919
24. Wotton, J. C., and Federhen, S. (1996) *Methods Enzymol.* **266,** 554–571
25. Walker, D. R., and Koonin, E. V. (1997) *Intelligent Syst. Mol. Biol.* **5,** 333–339
26. Notredame, C., Higgins, D. G., and Heringa, J. (2000) *J. Mol. Biol.* **302,** 205–217
27. Cuff, J. A., and Barton, G. J. (2000) *Proteins* **40,** 502–511
28. Brooks, S. P. J., and Storey, K. B. (1992) *Anal. Biochem.* **201,** 119–126
29. Liu, H. J., Chang, B. Y., Yan, H. W., Yu, F. H., and Liu, X. X. (1995) *J. AOAC Int.* **78,** 736–744
30. Watanabe, K., Yamano, Y., Murata, K., and Kimura, A. (1986) *Nucleic Acids Res.* **14,** 4393–4400
31. Newton, G. L., and Javor, B. (1985) *J. Bacteriol.* 438–441
32. Hunt, J. B., Smyrniotis, P. Z., Ginsburg, A., and Stadtman, E. R. (1975) *Arch Biochem. Biophys.* **166,** 102–124
33. Maurizi, M. R., Pinkofsky, H. B., and Ginsburg, A. (1987) *Biochemistry* **26,** 5023–5031
34. Shapiro, B. M. and Ginsburg, A. (1968) *Biochemistry* **7,** 2153–2167
35. Hunt, J. B., and Ginsburg, A. (1980) *J. Biol. Chem.* **255,** 590–594
36. Herschlag, D., and Jencks, W. P. (1990) *Biochemistry* **29,** 5172–5179
37. Witmer, M. R., Palmieri-Young, D., and Villafranca, J. J. (1994) *Protein Sci.* **3,** 1746–1759
38. Abell, L. M., Schineller, J., Keck, P. J., and Villafranca, J. J. (1995) *Biochemistry* **34,** 16695–16702
39. Glusker, J. P. (1991) *Adv. Protein Chem.* **42,** 1–76
40. Francis, S. H., Turko, I. V., Grimes, K. A., and Corbin, J. D. (2000) *Biochemistry* **39,** 9591–9596
41. Bock, C. W., Katz, A. K., Markham, G. C., and Glusker, J. P. (1999) *J. Am. Chem. Soc.* **121,** 7360–7372
42. Mesecar, A. D., Stoddard, B. L., and Koshland, D. E. (1997) *Science* **277,** 202–206
43. Esnousf, B. M. (1997) *J. Mol. Graph.* **15,** 133–138